Evaluation and Validation of ELSA Model in Diesel Sprays: 3D Cavitating Nozzles Case

Sergio Hoyas[†], Antonio Gil[†], Pablo Fajardo[†], Dung Khuong-Anh[†*], and Frederic Ravet[‡]
[†] CMT-Motores Térmicos, Universitat Politècnica de València, Valencia 46022, Spain
[serhocal, angime, pabfape, ankh2]@mot.upv.es
[‡]Renault, 1 Avenue du Golf 78288, Guyancourt, France
frederic.ravet@renault.com

Abstract

Computational Fluid Dynamic (CFD) techniques have become one of the main tools in the design and development of diesel engines. There exist, however, some drawbacks and problems that must be overcome in the next years. One of the challenges is to predict accurately the couple between the flow inside the nozzle and the spray, including the primary break-up and the secondary atomization. In the last years, several authors have been developed the Eulerian-Lagrangian Spray Atomization (ELSA) model. ELSA model combines an Eulerian and Lagrangian descriptions by coupling these two methods properly. ELSA model also accounts for the modeling of droplets and their formation process, particularly in the dense spray region. The ELSA model for diesel spray modeling has been recently implemented and developed into Star-CD CFD commercial code. Author's effort was focused on a detailed validation and evaluation of the fuel injection in diesel engines using this last implementation. Spray atomization, spray formation and macroscopic characteristics of diesel spray behavior were investigated. The overall work has been conducted in non-evaporative conditions. As cavitation greatly affects to spray behavior and it is though that cavitating nozzles will be present in most of close future engines, this sort of configuration has been chosen for validation. Velocity profiles at the section area of the nozzle exit obtained from trusted and experimentally validated RANS internal flow simulation were used. Results have been validated again experimental data, mostly coming from CMT-Motores Térmicos institute. It was found that the ELSA model reproduces accurately the experimental results.

Introduction

The primary break-up and secondary atomization of liquid sprays are up to now not totally understood. In the case of diesel engines, the fuel spray occurs in a small chamber inside the combustion engine. The fuel comes from a tiny nozzle cross section (hundred micrometers) at very high pressure and everything happens at an extremely short time (few milliseconds). Regardless the reactive part of the processes, diesel spray study includes several fundamentals, and not totally resolved topics, as can be the spray structure itself, break-up and atomization processes, or the behavior of two-phase turbulent flows. Probably, one of the main problems is the lack of experimental techniques which can be used in the vicinities of the nozzle.

Computational Fluid Dynamic (CFD) techniques have become one of the main tools in the design and development of diesel engines. There exists, however, some drawbacks and problem that must be overcome in the next years. One of the challenges is to predict accurately the couple between the flow inside the nozzle and the spray, including the primary break-up and the secondary atomization. Fuel injection and spray characterization have been investigated thoroughly during the last decades and there exist many techniques to model diesel spray. Each one of these methods has its own advantages and disadvantages, mainly due to the fact that they focus in a particular region of the spray. The traditional Eulerian method performs well in the liquid phase while the Lagrangian drop method describes accurately the dispersed region. Transition between both zones is not particularly well resolved, mainly due to time and computational power restrains. The ELSA model combines Eulerian and Lagrangian descriptions by coupling these two methods properly. It accounts for the modeling of droplets and their formation process, particularly in the dense spray region. In the last years several authors have been developed the ELSA model [1], [2], and [3]. This algorithm has been recently implemented in CD-adapco Star-CD CFD code conducted together with Renault SA in the version 4.12 and it has been continuously enhanced since then.

Spray modeling are commonly applied in ideally non-cavitating condition. The code has been pre-validated previously under non-evaporative and non-cavitating conditions, showing an excellent agreement with experimental data [4], [5], and [6]. However, nowadays nozzles cavitate, and this plays a critical role in real applications, affecting heavily on the spray behavior. In the next section the cavitating nozzles used for this validation are presented, together with the experimental data characteristics. The numerical methods are presented in the following section and after that discussed. Last section is devoted to conclusions.

Experimental setup

The experimental data used in this project were obtained as part of a broader collaboration between Renault and CMT-Motores Térmicos. The only cavitating diesel injection nozzle characterized in this project was a Bosch injector, reference no., DLLA 145 PV3 192 805. A microscopic characterization of this nozzle is presented at Figure 1.

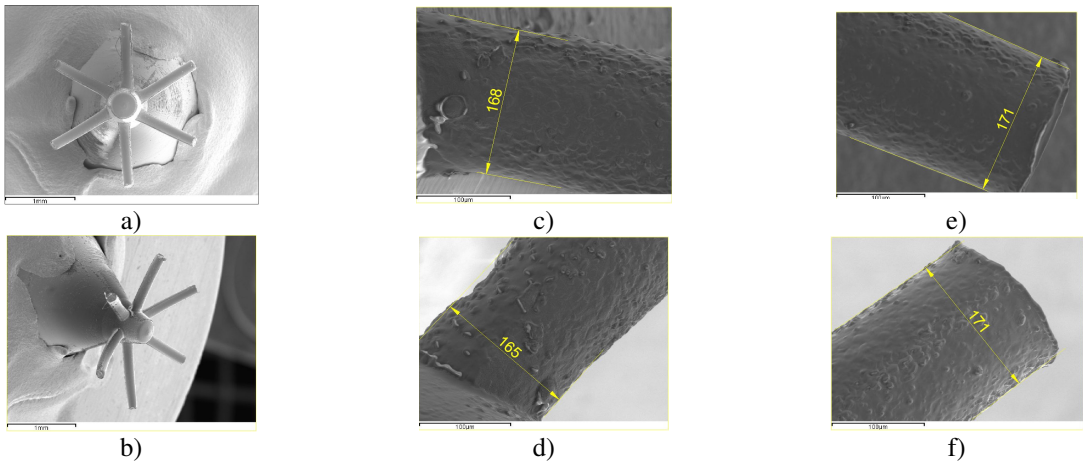

Figure 1: Detailed view of internal nozzle geometry.

Slightly differences in diameters were found amongst the six holes (Figure 1c, d, e, and f) so the mean diameter of the orifices has been used for the numerical analysis. This mean value is D_{Bosch} = 0.170 mm, 145º cone angle, *HE* = 13.5, and nozzle conicity, *k-factor* = 0.

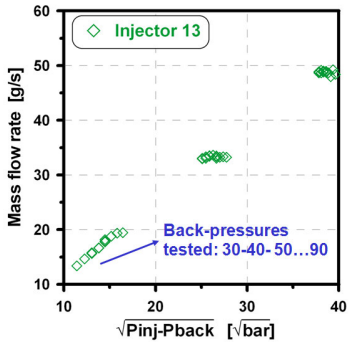

Figure 2: Mass flow rate vs. the variation between injection pressure and ambient pressure in the caviated injection nozzle (Injector 13).

The correlation amongst different injection pressure, back pressure vs. the mass flow rate obtained from experimental study is plotted in Figure 2. In this paper, the mass flow rate corresponded to a test case with the 30 MPa injection pressure and 7 MPa ambient pressure.

Computing the liquid length

The parameters linking the flow at the nozzle with the spray liquid length under evaporative condition were presented in [7], [8], [9] and [10]. According to the turbulent spray theory, in a quasi-steady spray, the fuel penetration is modeled by the following Eq.:

$$x = K_p \dot{M}_f^{\frac{1}{4}} \rho_a^{-\frac{1}{4}} t^{\frac{1}{2}} \tag{1}$$

Where ρ_a, is the ambient density, t is the time since the start of the injection (SOI). K_p is a function of the spray cone angle, θ_u.

$$K_p = k\left(\tan\left(\frac{\theta_u}{2}\right)\right)^{-\frac{1}{2}} \tag{2}$$

Where k is a universal constant, and K_p is the variable used in the fuel parcel penetration definition. The momentum flux, $\dot{M}_f$ is given in Eq. (3).

$$\dot{M}_f = \dot{m}_f u_{eff} = C_a \frac{\pi}{4} D_0^2 \rho_l C_V^2 u_{th}^2 \tag{3}$$

$$C_v = \frac{u_{eff}}{u_{th}} \tag{4}$$

$$u_{th} = \sqrt{\frac{2\Delta P}{\rho_l}} \tag{5}$$

In these equations, u_{eff} is the effective velocity, $\dot{m}_f$ is the fuel mass flow rate, C_a is the area coefficient, D_0 is the outlet diameter of the nozzle and ρ_l is the fuel density. The relationship between the effective velocity and the viscous-free theoretical velocity (u_{th} in Eq. (5)) is defined as C_v, (Eq. (4)). Delta pressure, ΔP is defined by $\Delta P = P_{inj} - P_{amb}$.

Substituting Eq. (3) into Eq. (1), the latter becomes

$$x = K_p \left(\frac{\pi}{4}\right)^{\frac{1}{4}} C_a^{\frac{1}{4}} C_o^{\frac{1}{2}} C_v^{\frac{1}{2}} u_{th}^{\frac{1}{2}} \rho_l^{\frac{1}{4}} \rho_a^{-\frac{1}{4}} t^{\frac{1}{2}} \tag{6}$$

The fuel parcel velocity in the axis, u_x is obtained deriving this equation, obtaining

$$u_x = \frac{\partial x}{\partial t} = K_p \frac{1}{2}\left(\frac{\pi}{4}\right)^{\frac{1}{4}} C_a^{\frac{1}{4}} C_o^{\frac{1}{2}} C_v^{\frac{1}{2}} u_{th}^{\frac{1}{2}} \rho_l^{\frac{1}{4}} \rho_a^{-\frac{1}{4}} t^{-\frac{1}{2}} \tag{7}$$

As spray momentum is a conserved magnitude:

$$\dot{M}_f = \dot{m}_f u_{eff} = \left(\dot{m}_f + \dot{m}_{a,x}\right) u_x \tag{8}$$

In this equation $\dot{m}_{a,x}$ is the air entrained by the spray. Defining C_m as the fuel mass fraction, from Eq. (8),

$$C_m = \frac{\dot{m}_f}{\dot{m}_f + \dot{m}_{a,x}} = \frac{u_x}{u_{eff}} \tag{9}$$

is obtaining. Replacing Eq. (7) to Eq. (9):

$$C_m = K_p . \frac{1}{2} . \left(\frac{\pi}{4}\right)^{\frac{1}{4}} . C_a^{\frac{1}{4}} . C_o^{\frac{1}{2}} . C_v^{-\frac{1}{2}} . u_{th}^{-\frac{1}{2}} . \rho_l^{\frac{1}{4}} . \rho_a^{-\frac{1}{4}} . t^{-\frac{1}{2}} \tag{10}$$

Using this equation it is possible to define a new time scale, t_m, defined as the time needed by a fuel parcel moving along the spray axis in order to reach a certain value of fuel mass fraction, C_m:

$$t_m = \frac{K_p^2 \frac{1}{4}\left(\frac{\pi}{4}\right)^{\frac{1}{2}} C_a^{\frac{1}{2}} D_O \rho_l^{\frac{1}{2}}}{C_m^2 C_v u_{th} \rho_a^{\frac{1}{2}}} \tag{11}$$

Using t_m, it is easy to compute the penetration distance, x_m, defined as the axial position with a "C_m" value of the fuel mass fraction.

$$x_m = \frac{K_p^2 \left(\frac{1}{4}\right)^{\frac{1}{2}} \left(\frac{\pi}{4}\right)^{\frac{1}{2}} C_a^{\frac{1}{2}} D_O \rho_l^{\frac{1}{2}}}{C_m \rho_a^{\frac{1}{2}}} \tag{12}$$

The liquid length (penetration), *LL*, is defined as the distance from the nozzle exit to the farthest location where the fuel parcel on the spray axis has entrained enough higher-temperature gas to vaporize the injected fuel. In order to obtain an equation for *LL*, C_m is taken equal to C_{mv} – the value of mass concentration in the axis at which the injected fuel is totally vaporized by higher-temperature gas.

By replacing the defined value of C_{mv} at Eq.(12) the liquid-phase penetration, *LL* is computed as *:*

$$LL = \frac{K_p^2 \left(\frac{1}{4}\right)^{\frac{1}{2}} \left(\frac{\pi}{4}\right)^{\frac{1}{2}} C_a^{\frac{1}{2}} D_O \rho_f^{\frac{1}{2}}}{C_{mv} \rho_a^{\frac{1}{2}}} \tag{13}$$

Numerical Study

Cavitation phenomena depends strongly on the nozzle geometry. In this particular case, cavitation occurs mostly on the upper part of the nozzle wall (see Figure 3).

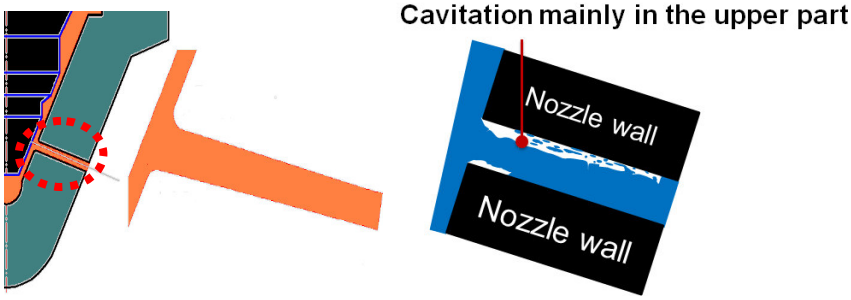

Figure 3: The nozzle, needle shape, and a zoom view of the internal nozzle flow (left) and the internal cavitation profile (right) produced by this type of injector.

The main physical parameters of the experimental set-up are tabulated in Table I.

Table I: The experimentally averaged parameters

Injection pressure	Ambient pressure	Momentum flow	Mass flow orifice	Effective velocity	Effective diameter	C_d	C_v	C_a
[MPa]	[MPa]	[N]	[g/s]	[m/s]	[μm]	[-]	[-]	[-]
30	7	0.540	18.79	172.5	166.9	0.706	0.733	0.963

To investigate the effects of diesel spray with the same cavitating nozzle, including or excluding cavitation phenomenon together with evaporative and non-evaporative conditions, three different cases, tabulated in table II, have been studied. In all cases, the injection pressure and ambient pressure were fixed to 30 MPa and 7 MPa respectively.

Table II: Computational cases

Case	D_0 (real diameter)	D_{eff} (effective diameter)	Nozzle cavitation	Inlet velocity	Evaporation	Ambient Temperature
	[µm]	[µm]	-	[m/s]	-	[K]
Case 1	170	165	Yes/simplify	V = 173	No	307.7
Case 2	170	-	Yes	Figure 5	No	307.7
Case 3	170	-	Yes	Figure 5	Yes	935.0

Effective velocity was rounded up to 173 m/s as described in case 1 of table II. To compensate for this increment, an effective diameter of 165 µm was used in the excluded-cavitating case. Figure 4a shows the output parameters extracted from the case with cavitation (case 2, and 3), whereas Figure 4b illustrates a simplified output parameters using in case 1 in which the cavitating nozzle is used but excluding the cavitating effects in simulation by using the effective values.

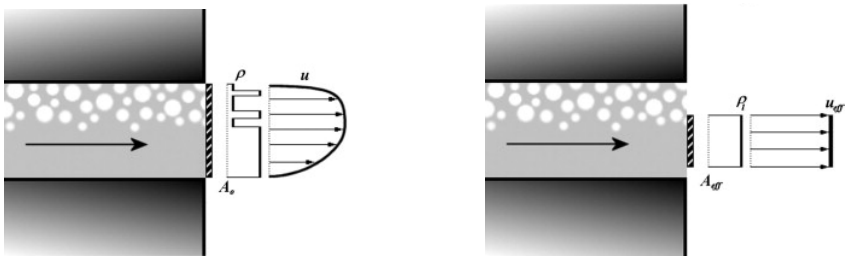

a) **b)**

Figure 4: The cavitated nozzle and its density, velocity profile including or excluding cavitation phenomenon [8].

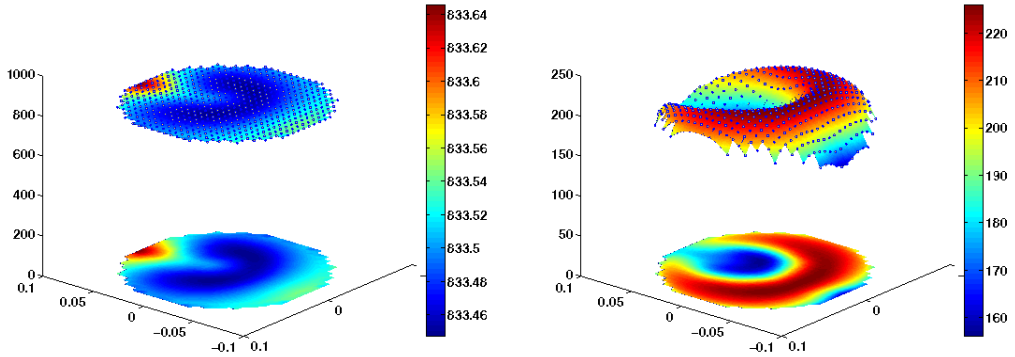

Figure 5: Density (on the left) and the velocity (on the right) at the nozzle exit (P_{inj} = 30 MPa, P_{amb} = 7 MPa, T_{amb} = 935 K).

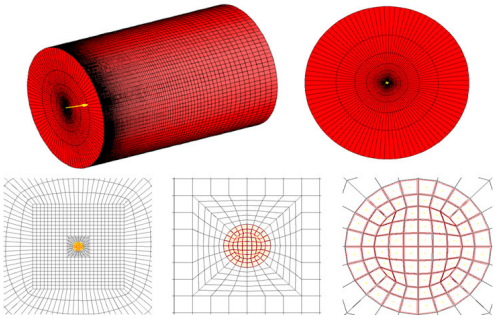

Figure 6: Computational mesh and detail of the grid structure near the nozzle exit (front view).

Taking into account the cavitating nozzle influence, the inlet boundary condition for case 2 and case 3 are shown in Figure 5. The cavitating modeling of the internal flow is seperatedly simulated by Salvador et al. using the open code, OpenFOAM. Thanks for the works of Salvador et al. 2010 [11] and 2011 [12]. A homogeneous

equilibrium model (HEM) was used and assumed that liquid and vapour phases are always perfectly mixed. Additionally, a barotropic equation of state was employed to model cavitation phenomenon (see more in [11] and [12]). The output data from internal flow calculation is extracted and interpolated in order to apply for the inlet boundary condition of the spray modeling. The effect of cavitation in the nozzle flow generated the variation at the cross-sectional nozzle exit as presented in Figure 5. The density and velocity profile distribution on the cross section are uneven.

About the geometry, in this study, only one nozzle of diameter 170 µm was simulated. The mesh, previously tested, is made of 518400 cells and 534877 vertices with 300 segments along the spray axis. This computational mesh and its structure are shown in Figure 6. Noted that a really fine mesh was built near the nozzle exit, and in the region where the spray developes . In this figure, the nozzle exit is the circular area containing 84 cells and bolding in red in the last two views of Figure 6. In the first case,where the simulate diameter is 165 µm, the length of all segments was scaled down by a coefficient of 165/170.

Results and Discussion

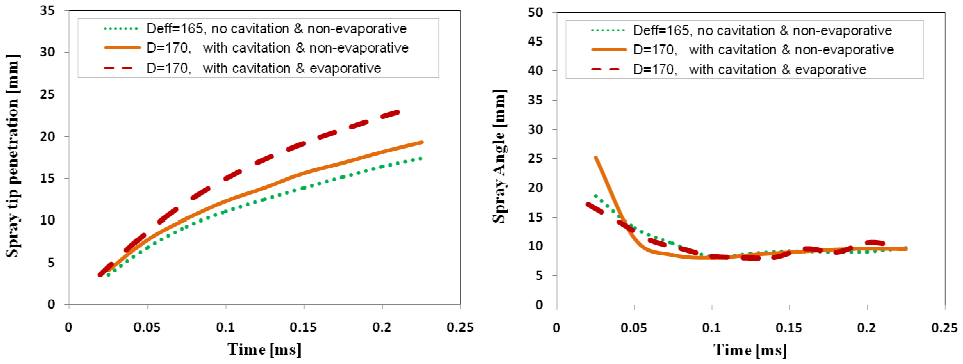

Figure 7: The comparison of the spray tip penetration and spray cone angle amongst three cases.

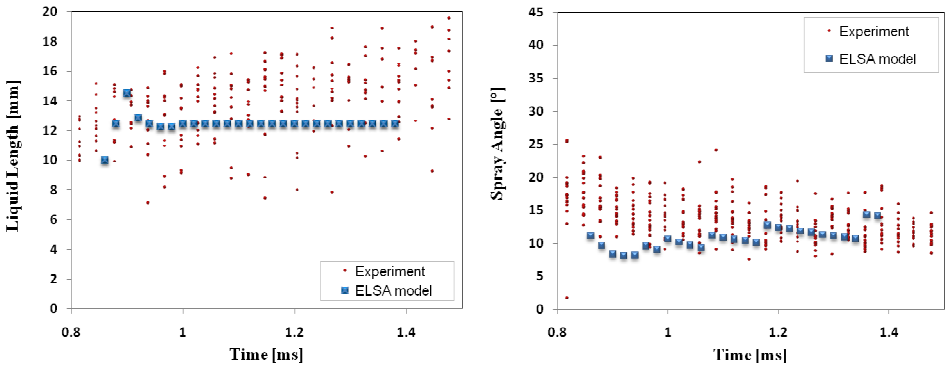

Figure 8: Comparison of experimental and numerical results in term of a) (left) liquid length and b) (right) spray cone angle under evaporative condition for the case with D= 170 µm, P_{inj} = 30 MPa, P_{amb}= 7 MPa, T_{amb}= 935 K.

In Figure 7, the spray tip penetration and spray cone angle of the three cases are shown. The spray tip penetration under cavitating and evaporative conditions – case 3 - was much higher than case 2, cavitating and non-evaporative conditions. It is also clear from these plots that the cavitation increases the spray penetration in comparison with the traditional simulation without cavitation, whereas the cone angle is similar in the three cases.

There also exist experimental results about the liquid length for the third case, showing an excellent agreement with the computed data, as it is shown in Figure 8a. Although there are a great dispersion in the data coming from the experimental (red dots) in Figure 8, the numerical results (blue dots) show a good agreement. As can be seen for the Figure 8b, the computed spray cone angle is a bit low at the beginning of the simulation, because we use as input the magnitudes coming from the steady region of nozzle, without simulating the transitory. The extracted data from the internal nozzle flow was taken only when the cavitation reached the certain stable value. That is also explained why we don't show the time before 0.8ms. Since the steady regime is reached, the agreement between experimental and numerical data is reasonably good.

Figure 9 expressed the effect of internal cavitating flow on the spray structure in both cross sections perpendicular to the spray axis as well as along the axial axis. The velocity contour at the cross section (perpendicular to the spray axis) taken at the position equal to one nozzle diameter from the nozzle outlet clearly shows the influence of cavitation phenomena on the spray formation. From this plot, the cavitation occurs mostly on the upper part of the nozzle wall (on the positive side of the Z axis) and there is very little variation on the X axis. As a consequent, the vapor mass fraction at the cross section along the spray axis on the XY plane is quite symmetric.

As depicted in the contour plots of the case 3 (Figure 10), two cross sections which are perpendicular to the spray axis at the distance of 5, and 10 mm has been extracted. The vapor mass fraction values were increased rapidly at the further distance. In every time step, there is a small vapor occurred in the area close to the nozzle diameter, that is at the section equal to 5 mm as liquid appears and the cavitating flow still heavily influent on the spray structure, however, the vapor mass faction obtained much more higher, it occupied whole section area at the distance of 10 mm where there is no more liquid. Under cavitation effects, the vapor mass fraction are asymmetric as observed clearly at 5 mm distance, once the sprays develop and the cavitation influence reduces at a longer distance the vapor mass fraction value tends more symmetric (refer to 10 mm at 0.08 ms). For case 1, and 2, since it simulated under non-evaporative conditions, the vapor mass fraction value are almost equal to zero at all cross sections and in every times step, thus, no it is no need to put it herein.

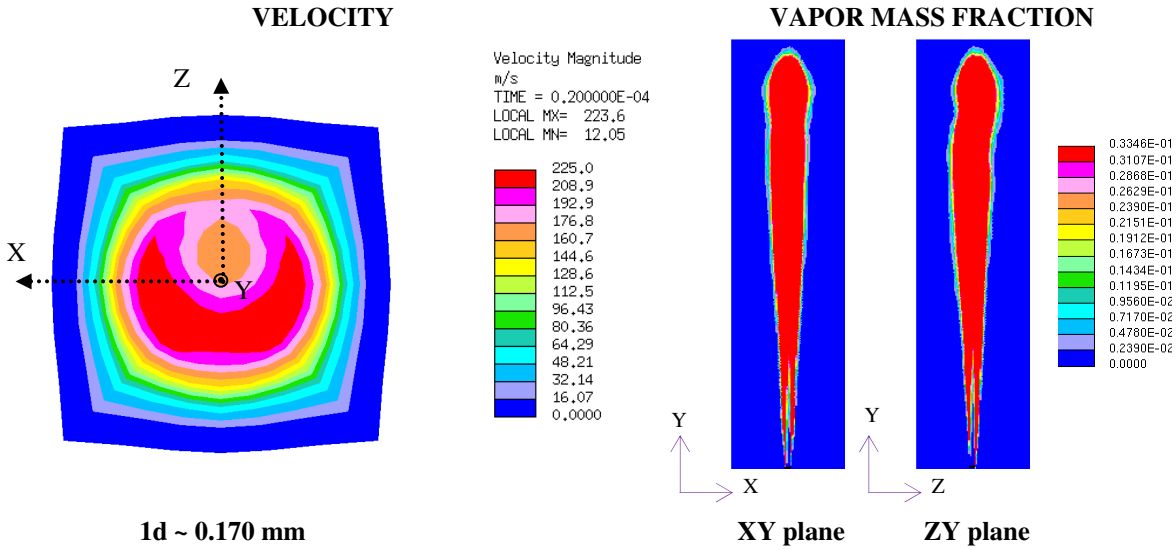

Figure 9: Velocity contour at 1D cross section (left), and vapor mass fraction profile along the spray axis in XY and ZY planes (two figures on the right hand side); contour plots of case 3 (P_{inj} = 30 MPa, P_{amb}= 7 MPa, T_{amb}= 935 K).

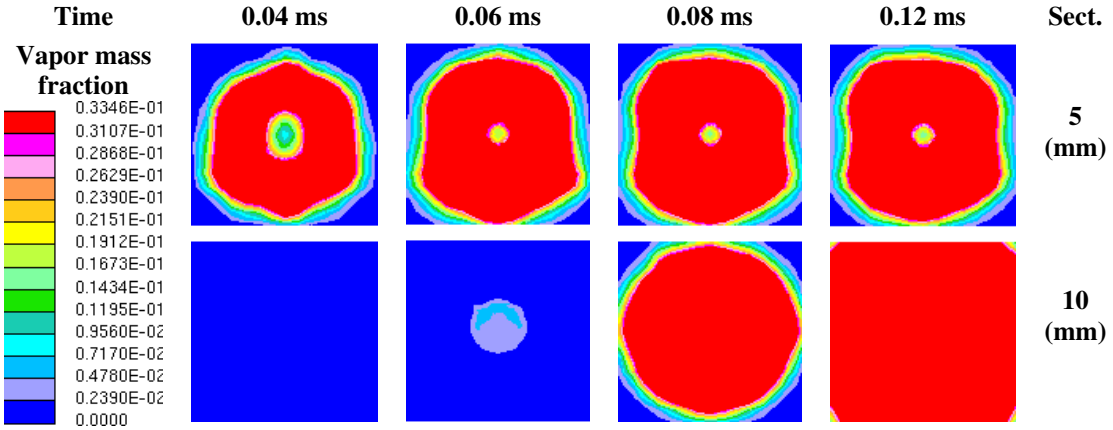

Figure 10: The vapor mass fraction at different cross sections [5, and 10 mm] along the spray axis and at different time steps [0.04, 0.06, 0.08, and 0.12ms] (D= 170 µm, P_{inj} = 30 MPa, P_{amb}= 7 MPa, T_{amb}= 935 K).

Summary and Conclusions

In this work the authors have presented a validation of the ELSA method implemented very recently in STAR-CD software. This study comprises three cases, combining cavitating nozzles in evaporative and non evaporative conditions. When possible the results have been compared to experiments, showing an excellent agreement. It is also important to notice that the spray tip penetration and spray cone angle in the cavitating nozzle cases are larger than in the case excluding cavitation. This probably made the spray more effective in the combustion stage.

Although a RANS model has been used to simulate turbulence, in order to take into account the effect of cavitation, a fine mesh has been used. The model produces also many droplets, so computation take a long time to run, even in parallel machines. This limited parametric study. As a future work, a more detailed parametric study is planned, including variation in ambient and injection pressure, ambient density and ambient temperature.

Acknowledgements

This work was supported in part by the Spanish Government in the frame of the Project 'Métodos LES para la simulación de chorros multifásicos', Ref. ENE2010-18542 and by Renault S.A. Experimental data was the joined project between Renault S.A., and CMT- Motores Térmicos. Dung Khuong-Anh has been also supported by the VECOM, EU FP7 Marie Curie Initial Training Network (ITN) Grant Agreement 213543.

References

[1] Vallet A, Burluka AA and Borghi R., *Atomization and sprays* 11: 619-642 (2001).

[2] Blokkeel G, Barbeau B and Borghi R., *SAE Technical Paper*: 2003-01-0005 (2003).

[3] Beau P.A. Modélisation de l'atomisation d'un jet liquide. Application aux sprays diesel. Ph.D. Thesis, *University of Rouen:* (2006).

[4] Hoyas, S., Pastor, J. M., Khuong-Anh, D., Mompó-Laborda, J. M., and Ravet, F., *International Journal of Vehicle Systems Modelling and Testing* 6-3/4: 187-201 (2011).

[5] Hoyas, S., Pastor, J. M., Khuong-Anh, D., Mompó-Laborda, J. M., and Ravet, F., *SAE Technical Paper:* 2011-37-0029 (2011).

[6] Hoyas, S., Gil, A., Margot, X., Khuong-Anh, D., and Ravet, F., *Mathematical and Computer Modelling* (2011).

[7] Payri, R., Salvador, F.J., Gimeno, J. and Zapata, L.D. *Fuel* 87: 1165-1176 (2008).

[8] Payri, R., Salvador, F.J., Gimeno, J. and De la Morena, J., *International Journal of Heat and Fluid Flow* 30-4: 768-777 (2009).

[9] Payri, F., Bermúdez, V., Payri, R., and Salvador, F., *Fuel* 83: 419 - 431 (2004).

[10] Desantes, J.M., Payri, R., Garcia, J.M., and Salvador, F.J., *Fuel* 86: 1093-1101 (2007).

[11] Salvador, F.J., Romero, J.V., Roselló, and M.D., Martínez-López, *Mathematical and Computer Modelling 52*, 1123-1132 (2010).

[12] Salvador, F.J, Hoyas, S., Novella, and R., Martínez-Lóper, *Proceedings of the Institution of Mechanical Engineers, Part D: Journal of Automobile Engineering* 225, 545-563 (2011).

[13] Hiroyasu H. and Arai M., *SAE Technical Paper:* 900475 (1990).

Appendix: Nomenclature

C_m	fuel mass concentration in the spray axis	t	time elapsed from the start of the injection
C_{mv}	fuel mass concentration in the spray axis to evaporate the fuel	T_a	temperature in the engine injection chamber
k-factor	nozzle conicity	u_{eff}	effective velocity at the outlet orifice
k	constant used in the fuel parcel penetration definition	u_{th}	theoretical velocity at the outlet orifice
K_p	variable used in the fuel parcel penetration definition	u_x	velocity of a fuel parcel in the axis of a stationary spray
LL	liquid-length	x	penetration of a fuel parcel in the axis of a stationary spray
$\dot{M}_f$	momentum flux at the nozzle outlet orifice	x_m	spray axial position where a mass fuel concentration equal to C_m is located
$\dot{m}_a$	mass flow rate of air entrained by the spray	***Greek symbols***	
$\dot{m}_f$	fuel mass flow rate	ΔP	Delta Pressure, $\Delta P = P_{inj} - P_{amb}$
P_{amb}	ambient pressure / back pressure	ρ	density
P_{inj}	injection pressure	ρ_a	ambient density
t_m	time needed for a fuel parcel in the axis of a stationary spray in order to reach a concentration equal to C_m	ρ_l	fuel density
		θ_u	spray cone angle